Available online at www.sciencedirect.com
ScienceDirect
Tectonophysics 424 (2006) 367–376
TECTONOPHYSICS
www.elsevier.com/locate/tecto

Forecasting rupture dimension using the pattern informatics technique

K.F. Tiampo [a,*], J.B. Rundle [b,1], W. Klein [c], J.R. Holliday [b,1]

[a] Department of Earth Sciences, University of Western Ontario, London, ON, Canada
[b] Center for Computational Science and Engineering and Department of Physics, University of California, Davis, CA, USA
[c] Department of Physics, Boston University, Boston, MA, USA

Received 22 July 2005; received in revised form 26 November 2005; accepted 25 March 2006
Available online 22 June 2006

Abstract

The Pattern Informatics (PI) technique [Tiampo, K.F., Rundle, J.B., McGinnis, S., Gross, S., Klein, W., 2002. Mean-field threshold systems and phase dynamics: An application to earthquake fault systems, Europhys. Lett., 60, 481–487] is founded on the premise that changes in the seismicity rate are a proxy for changes in the underlying stress. This new approach to the study of seismicity quantifies its local and regional space–time patterns and identifies regions of local quiescence or activation. Here we use a modification of the PI method to quantify localized changes surrounding the epicenters of large earthquakes in California in an attempt to objectively quantify the rupture zones of these upcoming events. We show that this method can be used to forecast the size and magnitude of future earthquakes.

Keywords: Seismicity; Stress; Earthquake physics; Seismic hazard

1. Introduction

Recent work by Rundle et al. (2000) and Tiampo et al. (2002) produced a new approach to the study of seismicity, the pattern informatics (PI) technique, a methodology for quantifying the spatiotemporal seismicity rate changes in historic seismicity. Recognizing that the seismicity rate is proportional to the stress change rate, and thus systematic space–time variations in seismicity occur in response to changes in the underlying stress field (Dieterich, 1994; Dieterich et al., 2002; Toda et al., 2002), the PI methodology therefore quantifies the underlying stress change in terms of the change in seismicity rate relative to the background seismicity (Tiampo et al., 2002).

In addition, research that interprets seismicity as the surface expression of a system near a critical point suggests that correlated regions of varying spatial dimensions should exist for some period of time (Jaume and Sykes, 1992; Main, 1996; Bowman et al., 1998; Huang et al., 1998). In related work, it has been shown that the earthquake fault system behaves as a mean-field threshold system, with correlated regions on the order of several hundred kilometers in radius and nucleating droplets around which these events coalesce (Klein et al., 1997; Bowman et al., 1998; Tiampo et al., 2003). If they could be identified, these smaller

* Corresponding author. Tel.: +1 519 661 3188.
E-mail addresses: ktiampo@uwo.ca (K.F. Tiampo), jbrundle@ucdavis.edu (J.B. Rundle), klein@buphyc.edu (W. Klein).
[1] Tel.: +1 530 752 6416.

0040-1951/$ - see front matter © 2006 Elsevier B.V. All rights reserved.
doi:10.1016/j.tecto.2006.03.047

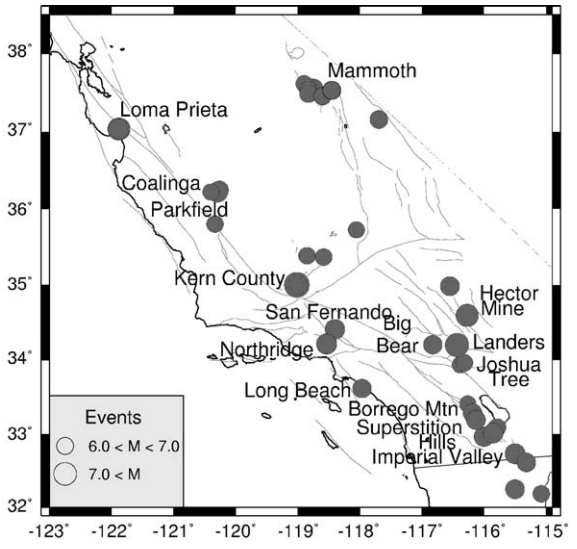

Fig. 1. Locations of significant events in California, 1932–2000.

nucleation zones should act as precursors for the largest events in the fault network. In addition, we hypothesize that these areas should also delineate the physical region of stress concentration, and therefore the upcoming rupture zone.

For this work, we employ the PI method to identify preliminary areas of study in the California fault network. Fig. 1 shows a plot of the largest events to occur in central and southern California since 1932. Once these preliminary locations of increased likelihood of an event are identified, we attempt to determine the size of the upcoming earthquake by quantifying its rupture length. In California, with its relatively shallow, fixed seismogenic depth, earthquake magnitude is generally a function of the total length of the fault break, and empirical relations have been determined that allow for the calculation of magnitude given fault length (Wells and Coppersmith, 1994). Here we show that the rupture dimension for large events can be determined using a variation of the PI technique, allowing for a first order calculation of the magnitude of the forecast earthquake.

2. Methodology

In phase dynamical systems, the space–time evolution of the system can be described by changes in the amplitude and phase angle of a state vector, or phase function (Mori and Kuramoto, 1998). Computer simulations strongly suggest that earthquake seismicity can be described by phase dynamics, in which the important changes in seismicity are associated only with rotations, or changes in phase angle, of the vector function that describes the seismicity in a high-dimensional correlation space (Rundle et al., 2000; Tiampo et al., 2002). Here, space–time pattern structures are non-local in character, a consequence of the strong correlations in the underlying dynamics, where non-local means that events widely separated in space and time may be correlated with each other.

The PI procedure we apply here is based upon the idea that seismic activity is characterized by a vector or phase function, $\hat{\mathbf{S}}$. Changes in the state of seismicity in space and time, or the change in stress rate, are characterized by changes in $\hat{\mathbf{S}}$. It should be noted that we have performed the same calculation for seismic moment, and the results are similar, but the assignment of moment to the events adds another source of error to the calculation. As a result, we have confined our recent work to quantifying the numbers of events.

Define the seismic activity rate $\psi_{\mathrm{obs}}(x_i,t)$ as the number of earthquakes per unit time, of any size greater than a given magnitude cutoff, within the box centered at x_i at time t. We define the time-averaged seismicity function $\mathbf{S}(x_i,t_0,t)$ over the interval $(t-t_0)$:

$$\mathbf{S}(x_i,t_0,t)=\frac{1}{(t-t_0)}\int_{t_0}^{t}\psi_{\mathrm{obs}}(x_i,t)\mathrm{d}t\cdot \tag{1}$$

Since there are N locations for $\mathbf{S}(x_i,t_0,t)$, and we assume t_0 to be a fixed time, $\mathbf{S}(x_i,t_0,t)$ is the i-th component of a general, time-dependent vector evolving in an N-dimensional space. Denoting spatial averages over the N boxes by $<>$, the phase function $\hat{\mathbf{S}}(x_i,t_0,t)$ is then defined to be the mean-zero, unit-norm function obtained from $\mathbf{S}$:

$$\hat{\mathbf{S}}(x_i,t_0,t)=\frac{\mathbf{S}(x_i,t_0,t)-<\mathbf{S}(x_i,t_0,t)>}{||\mathbf{S}(x_i,t_0,t)||}, \tag{2}$$

where $||\mathbf{S}(x_i,t_0,t)||$ is the square root of the variance (the standard deviation) over all spatial boxes.

Under the assumption of phase dynamics, the important changes in seismicity will be given by $\Delta\hat{\mathbf{S}}(x_i,t_1,t_2)=\Delta\hat{\mathbf{S}}(x_i,t_0,t_2)-\Delta\hat{\mathbf{S}}(x_i,t_0,t_1)$, a rotation of the N-dimensional unit vector $\hat{\mathbf{S}}(x_i,t_0,t)$ in time. The PI index at x_i, $\Delta\mathbf{P}(x_i,t_1,t_2)$, from time t_1 to t_2, is then

$$\Delta\mathbf{P}(x_i,t_i,t_2)=\{\Delta\hat{\mathbf{S}}(x_i,t_i,t_2)\}^2-\mu_P, \tag{3}$$

where μ_P is the spatial mean of $\{\Delta\hat{\mathbf{S}}(x_i,t_1,t_2)\}^2$. Note that rotations in $\hat{\mathbf{S}}(x_i,t_0,t)$ correspond to a change in the local rate of seismicity, or number of events, normalized to a regional background rate, resulting in an objective measure of the changing seismicity rate and, as a result,

the changing stress state (Dieterich, 1994; Tiampo et al., 2002).

Fig. 2a shows a plot of $\Delta\hat{\mathbf{S}}$ for the years 1989 to 1999. The primary seismicity data set used to calculate $\Delta\hat{S}$ in this figure is a compilation catalog from 1932 through the end of 1999, obtained from the Southern California Earthquake Center (SCEC) database (available at http://www.scecdc.scec.org.) and the Northern California Seismic Network (NCSN, http://quake.geo.berkeley.edu/ncsn/), with all blast events removed. A positive (red) value represents anomalous seismic activity, and a negative (blue) value of represents anomalous quiescence. Fig. 2b shows the corresponding PI index, $\Delta\mathbf{P}(x_i,1989,1999)$, where the color scale is now logarithmic, with the number denoting the exponent to the base 10. Fig. 2b was originally published by Rundle et al. (2002), as a test of the PI methods ability to forecast large events greater than $M\sim5$ during the period 2000 to 2010. To date, 16 of 18 events of magnitude five or greater that have occurred since January 1, 2000 have fallen within one box dimension of a PI anomaly shown on this map. In recent work, Holliday et al. (2005) demonstrate using a forecast verification technique (Joliffee and Stephenson, 2003) similar to that of Molchan (1997), that the results of this forecast through the first 5 years of testing are significant. This particular verification methodology is based upon the hypothesis that the PI forecasts are binary forecasts, i.e. that there will be an earthquake for any PI value above some given threshold (Holliday et al., 2005, in press). Fig. 3 shows these results, based upon a comparison between the original PI analysis as shown in Fig. 2 (Tiampo et al., 2002) and a relative intensity (RI) measure computed from background seismicity, over all possible threshold values (Holliday et al., 2005). Confidence intervals are as computed by Zechar and Jordan (2005). Fig. 3 demonstrates that the PI index does consistently better than the RI index for most threshold values, and is significant at the three-sigma level when compared to random guessing.

These recent developments suggesting that the PI index represents a threshold probability, in which a value may be chosen above which there is 100% expectation of a large event, provide the basis for modifications to the PI calculation. Here we identify those smaller regions where the PI value reaches extremely high local values, and thus can be used to delineate the fault rupture zone. The primary seismicity data set used to calculate $\Delta\hat{S}$ for central and southern California employed in this analysis is as in Fig. 2. Relevant data include location, in latitude and longitude,

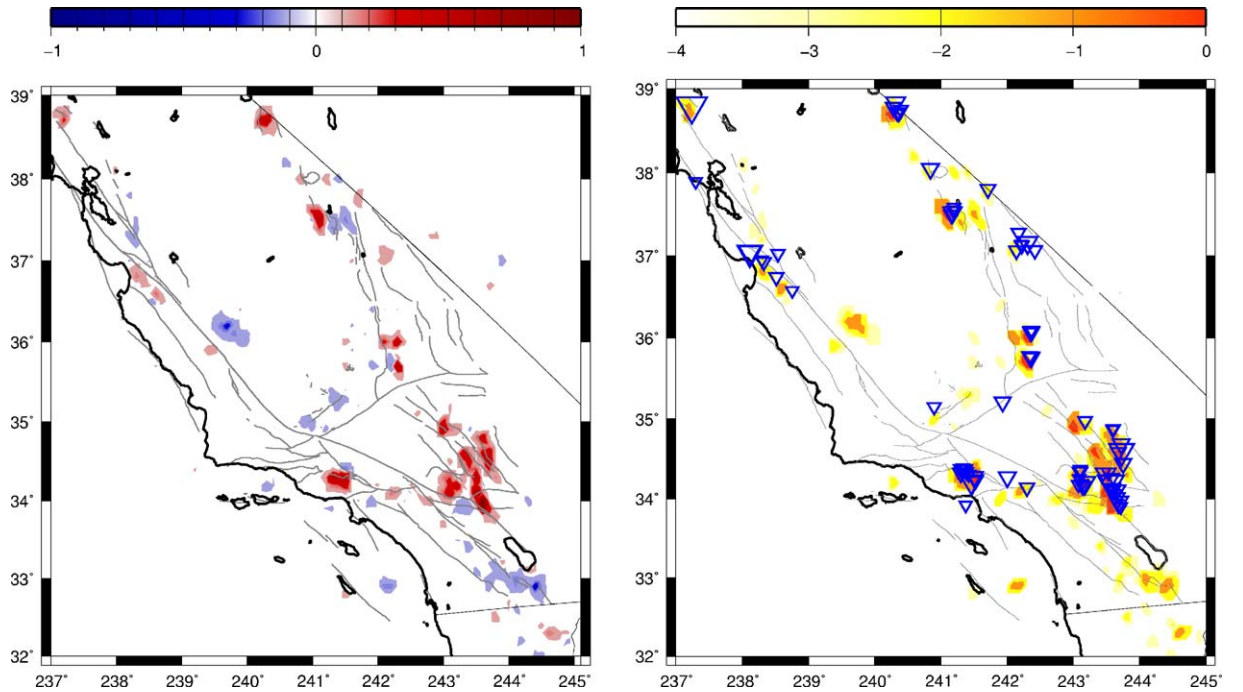

Fig. 2. a) Map of $\Delta\mathbf{S}$, normalized to the maximum absolute value, for the time period 1999–1989. The color scale is linear, blue to white to red; and b) color contour plot of PI index, $\Delta\mathbf{P}$, for locations at which $\Delta\mathbf{P}>0$, 1999–1989. Color scale is logarithmic, where the number represents the exponent. Inverted triangles are events that occurred from 1999–1989 for events of $5<M$ (triangle size scales with magnitude).

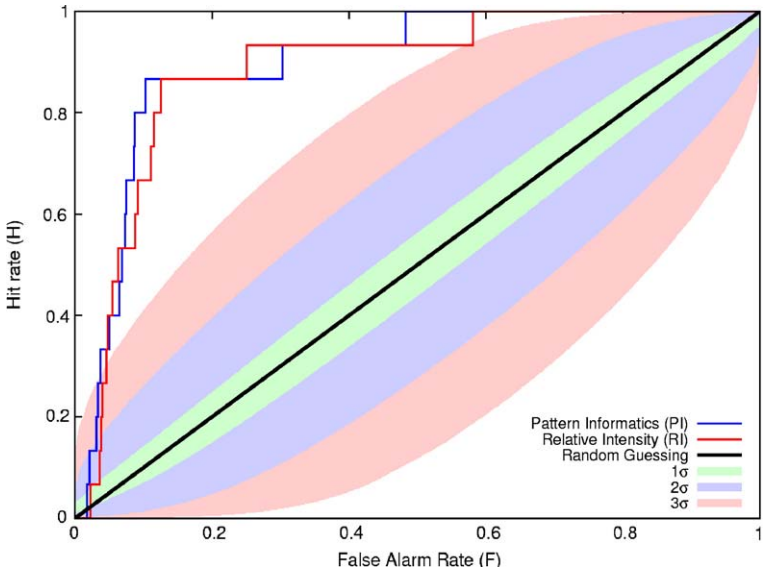

Fig. 3. Relative operating characteristic (ROC) diagram. Plot of hit rates, H, versus false alarm rates, F, for the PI forecast (blue), RI forecast (red), and random guessing (black). Confidence intervals for the one-, two- and three-sigma levels are shown as well (Holliday et al., 2005; Zechar and Jordan, 2005).

and the time the event occurred. Seismic events between −115° and −125° longitude and 32° and 40° latitude were selected, and events of all quality were acquired. The seismicity was binned into squares of 0.1° latitude and 0.1° longitude to a side, approximately 11 km to a side, and a magnitude cut of 3.0 was applied to the data.

We begin by taking small subsets of the California fault zone, each centered on a particular, known epicenter. These sub-regions begin at a small but reasonable size, on the order of 0.1 to 0.4°, and they increase systematically, again in steps of 0.05 to 0.2. The PI calculation is then performed for each of these sub-regions. Fig. 4 illustrates, schematically, this procedure for the Landers epicenter. Fig. 4a illustrates the various increasing box sizes superimposed on each other, while Fig. 4b and c show the individual, increasing regions actually used in the calculation. Again, we do not take any seismicity that occurs after the actual event. The box size for the gridding of the seismicity and the calculation of the PI index remains separate, as detailed above, and can be different from the sub-region size or its increasing step size.

In this particular variation of the PI index, here denoted the roughness index, we do not normalize the PI values to the maximum, as done in Fig. 2 for plotting purposes. In initial studies, it was observed that the PI values for those smallest sub-regions that encompass the upcoming event are very high, on the order of tens to thousands. Based on the discussion above, that the PI index is a binary forecast, quantifying, based on a threshold level, whether an event will or will not occur in the future, we wish to evaluate these smaller sub-regions based upon whether they exceed a particular threshold. That threshold was set at a value of 1.0, i.e. rupture is a certainty if the value in the box is above 1.0, and all values of the PI index in that region that are greater than 1.0 in the original calculation then are set equal to 1.0. This particular value was chosen based upon those early studies, when we examined the statistical distribution of the PI values over the entire region, and determined that low level fluctuations existed below a PI value of 1.0. Subsequently, the mean and variance of the PI values in each gridded box location is calculated for these sub-regions, over all potential sub-regions.

3. Results

Fig. 5 shows the mean and variance of the roughness index calculated for each increasing region size (shown schematically in Fig. 4) around the epicenter of the Landers earthquake of 1992, for a 10-year period prior to the earthquake (1981–1991). In this case, the initial region size is a box of side 0.4°, and each subsequent box dimension increases by 0.4°. The roughness value is calculated for each of the separate grid locations, box sizes of 0.1° to a side as above, for every sub-region steps. The solid line represents the mean of those values, calculated for every gridded location. The calculation only includes those boxes for which there is a value

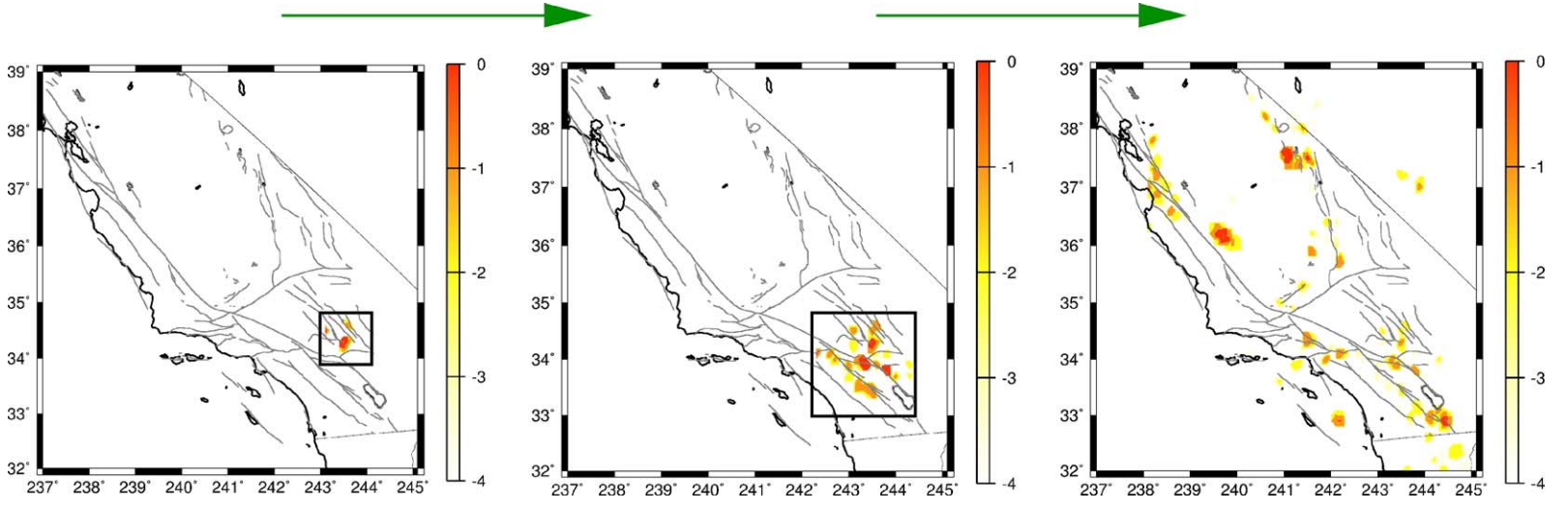

Fig. 4. The above illustrates the technique used to quantify the PI index for varying sub-regions around the Landers epicenter. The increasing sub-region sizes are illustrated, grouped around the Landers epicenter. The actual calculation is performed for each sub-region alone, as shown in a), b) and c). Color bar is as described in Fig. 2b.

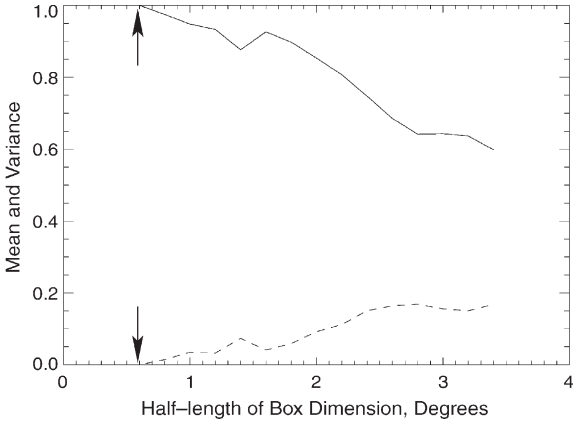

Fig. 5. The mean and variance of the roughness value calculated for increasing region size around the epicenter of the Landers earthquake of 1992, for a 10-year period prior to the earthquake (1981–1991). The solid line represents the mean of that value for a region circumscribed by a box with a half-length dimension shown on the *x*-axis. The dashed line is the variance of the roughness value for that same box dimension. Here the box dimension was increased in steps of 0.2°, and the rupture half-length is marked by arrows. Seismicity used for this calculation ends in 1991.

greater than zero, hence the similarity to a roughness calculation. On the *x*-axis is the half-length dimension of the box that circumscribes each region, in degrees. The dashed line is the variance of the roughness index for that same sub-region size.

Note here that there is a region that is centered at the epicenter of the Landers earthquake for which the mean of the roughness value remains one while the variance is zero. This dimension is approximately 66 km, given that 0.1° is equal to approximately 11 km in southern California. This particular length is roughly the order of the known subsurface rupture dimension for the Landers earthquake, as shown in Table 1.

Table 1
Source dimension, select CA earthquakes

Event	Year	Magnitude	Rupture dimension (km)	Reference
Borrego Mountain	1968	6.5	40	Wells and Coppersmith, 1994
Coalinga	1983	6.4	15	Beresnev and Atkinson, 2002
Palm Springs	1986	5.6	16	Wells and Coppersmith, 1994
Loma Prieta	1989	7.1	40	Wells and Coppersmith, 1994
Landers	1992	7.3	80	Hauksson et al., 1993
Northridge	1994	6.7	10–30	Hauksson et al., 1995

However, the dimension shown on the *x*-axis of Fig. 5 is the *half-length* of this region in which the PI index is very high. Any calculation for the total rupture dimension must be doubled, resulting in a value of approximately 132 km, too long for the initial event in the Landers sequence. As a result, we investigate the actual spatial variation of these values in Fig. 6.

Fig. 6 shows the roughness index for the region size corresponding to a total dimension of 1.2°, or 132 km. This is the region from Fig. 5 in which all values of the roughness index are either 1.0 or zero, and the mean of the roughness index equals 1.0. In this figure the roughness index appears to delineate not just the upcoming Landers earthquake, but the entire Landers sequence, including the Joshua Tree earthquake of 1992 to the south. In addition, this is a forecast for the time period 1992 to 2002, so that the Hector Mine event of 1999 is highlighted to the north as well. The total rupture dimension calculated in Fig. 5 is for all three events, approximately 2/3 of which, or 88 km, can be attributed solely to the Landers earthquake (Hauksson et al., 1993).

Calculation of the roughness index for the Borrego Mountain earthquake of 1968 and the Loma Prieta earthquake of 1989 was performed as well. For these, and all subsequent roughness calculations, the seismicity catalog for the calculations is terminated in the year prior to the event itself. Here the calculation is performed as in Fig. 5, and again there exists a region centered on the epicenter of each event where the mean

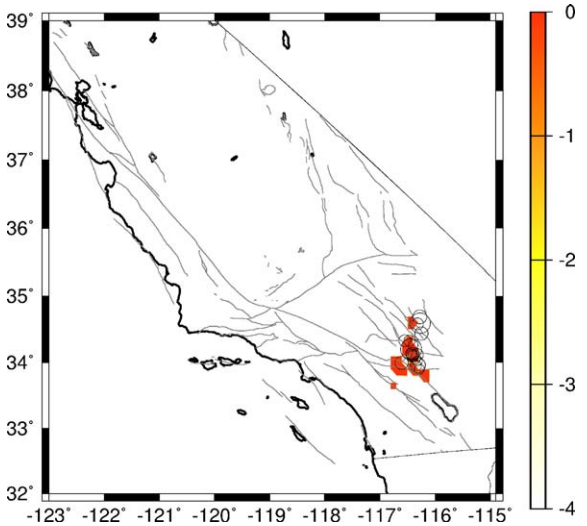

Fig. 6. The roughness index for the region size delineated in Fig. 5, a box 1.2° per side. All colored values equal 1.0. Circles are events for that rupture length that occurred from 1992–present, again for $5<M$ (circle size scales with magnitude).

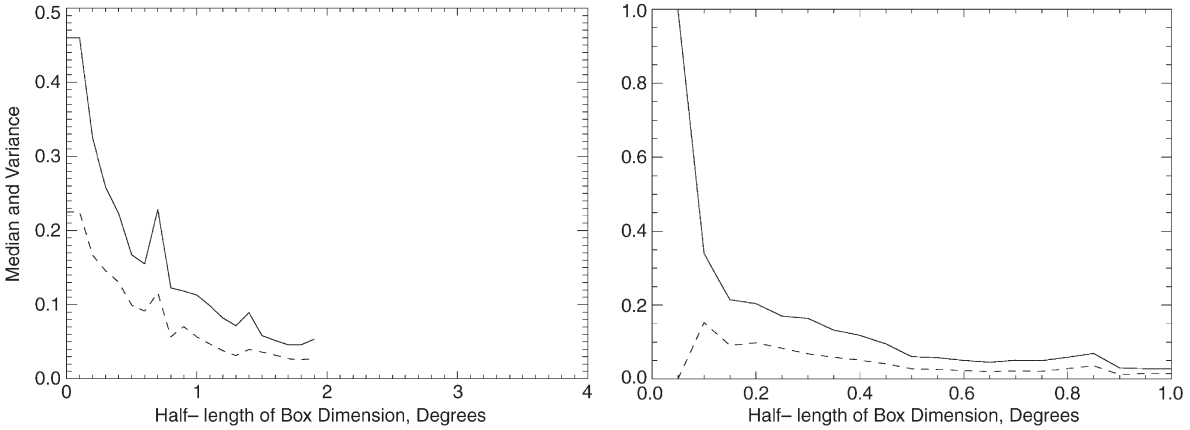

Fig. 7. a) The mean and variance of the roughness calculations for region sizes centered at the Coalinga earthquake of 1983, for step increases in region size of 0.1° to a side and b) the same calculation, at the Coalinga epicenter, for increases of 0.05° in each box size. Seismicity for the calculation ends in 1982.

of the roughness index is a constant that equals 1.0 and the variance equals zero. For both of these events the associated rupture dimension is less than 44 km, twice the dimension along the *x*-axes (Wells and Coppersmith, 1994). These values match reasonably well with those values given in Table 1, given the discretization inherent in this calculation.

This discretization occurs in two locations in the calculation. The first is in the box sizes that we decimate the seismicity catalog into for the initial PI calculation, and the second enters in through the increasing step size of the sub-regions. These effects are illustrated in Fig. 7, which shows the mean and variance of the roughness index for the Coalinga earthquake of 1983. The subsurface rupture of this reverse thrust event was on the order of 15 km, smaller than the initial region size of 0.4°, or 44 km, chosen for the earlier calculations. Fig. 7a shows, therefore, the calculation starting with an initial sub-region size of 0.2°, where the sub-region size increases by 0.1° to a side for every increment, and the initial PI calculation is gridded into box sizes of 0.1°. Note that, even at this smaller size, there is variation in the roughness index at the smallest region size.

Fig. 7b shows the calculation for an initial sub-region size of 0.1°, a step size of 0.05°, and a gridding of the historic seismicity into a box size of 0.05°. There is delineated a smooth region size of 0.05° in half-length, corresponding to a rupture dimension of approximately 11 km, on the order of that shown for the Coalinga earthquake in Table 1 (Beresnev and Atkinson, 2002).

As a result, for the additional two smaller events of Table 1, the North Palm Springs event of 1986 and the

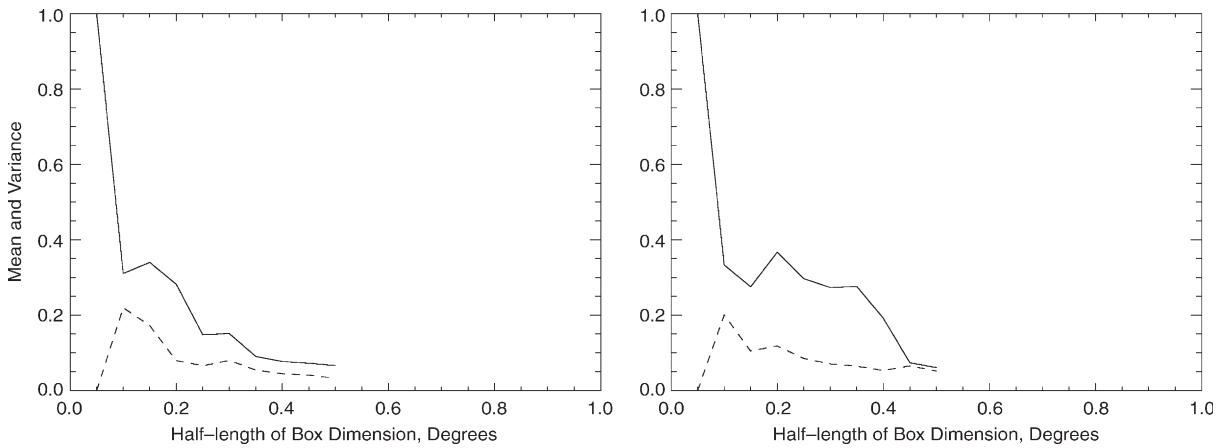

Fig. 8. Roughness calculation a) centered at the epicenter of the North Palm Spring earthquake of 1986 and b) centered at the epicenter of the Northridge earthquake of 1994. Here the region of calculation is increased in steps of 0.05°. Seismicity for the plot in a) ends in 1985; seismicity for b) ends in 1993.

Northridge event of 1994, the roughness index was calculated as in Fig. 7b. Fig. 8a shows the result for the North Palm Springs earthquake, and results in an approximate rupture dimension of 11 km, which compares well to the 16 km generally attributed to the event (Wells and Coppersmith, 1994). Fig. 8b also delineates an approximate rupture dimension of 11 km for the Northridge earthquake, again a value that compares well to that given in the literature. The value for this particular earthquake given in Table 1 is a result of the fact that the subsurface rupture length varied significantly with depth (Hauksson et al., 1995).

Finally, in Fig. 9, we test one appropriate null hypothesis. To ensure against the possibility that natural variation in the local seismicity is causing the phenomena seen in the earlier figures, and is not specifically associated with an upcoming event, we selected a random location and year for which the only requirement was that there should be no subsequent large event in the catalog at that location. The particular location is shown in Fig. 9a, and the year is 1988. The roughness index has been calculated for this site, for box sizes of 0.1° and increments of both 0.1 and 0.2°, and no coherent region with a constant mean of 1.0 and a variance of zero is delineated, as shown in Fig. 9b. While there does appear to be a coherent region at a distance of approximately 0.3° from the random location chosen initially, if we examine this phenomena by moving the center of a new analysis to that location, another site with no large earthquake after 1988, no coherent region emerges either. This suggests that the region detected by this variation of the PI method is associated with the upcoming events, not the result of random fluctuations in seismicity, and that it is related to this phenomena of small, coalescing regions that are linked to the rupture zone (Klein et al., 1997).

4. Discussion and conclusions

From the analysis above, it can be seen that the PI index has the potential to provide not only intermediate-term forecasts of the locations for upcoming earthquakes, but may also be able to quantify the magnitude of these events. This gives additional, significant insight into the method. In looking at Fig. 2, for example, it was not possible, simply by examining the normalized values, to determine the magnitude of the upcoming events. In other words, the intensity of the anomalies in Fig. 2 is not necessarily a guide to the size of the associated earthquakes. With the accurate determination of the rupture dimension using the roughness index, that magnitude calculation can be made for the entire California fault system, using empirical estimation methods as found in Fig. 14 of Wells and Coppersmith (1994).

Note that, while the rupture dimensions calculated here are in good accordance with those shown in Table 1, their correct quantification depends on both the box size of the initial PI calculation, and the step size increase in the sub-region size. Therefore, to calculate this dimension correctly, the smallest possible size should be chosen for both. For example, for the Coalinga, North Palm Springs, and Northridge events shown above, the rupture dimension is only given to an order of magnitude. To define a more exact rupture length, it would be necessary to reduce both dimensions

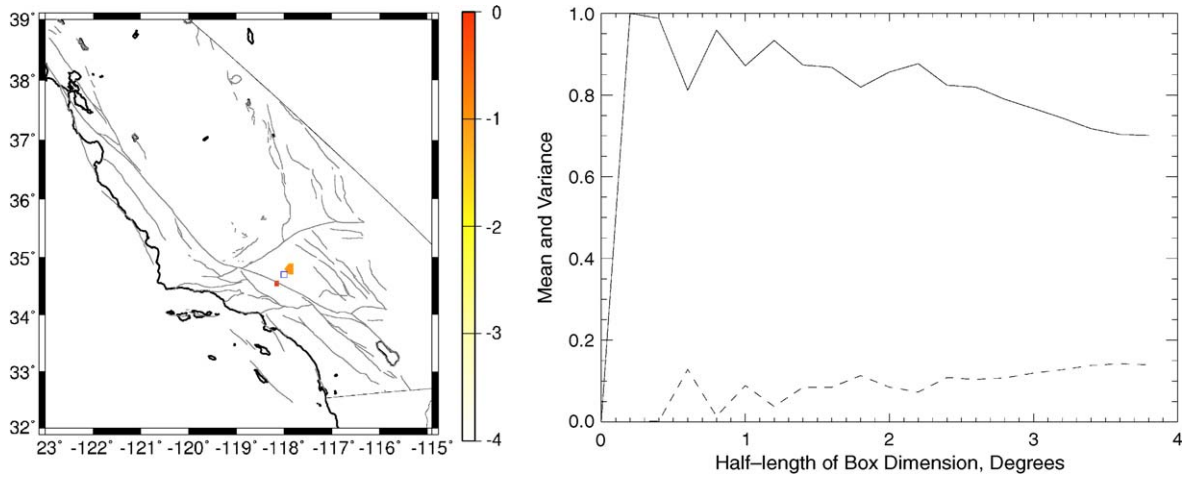

Fig. 9. The roughness calculation for a random location and year, in this case 1988. No large earthquake has occurred at the location shown in a) since that time. The calculation for an increasing region size of 0.1° is shown in b).

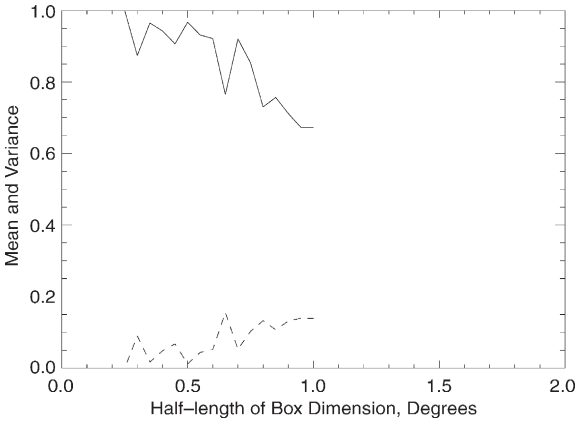

Fig. 10. The roughness calculation for 35.9° latitude, 120.5° longitude, as of 1999. This corresponds to the location of the associated PI anomaly shown in Fig. 2b, for the same time period. The calculation is made for a PI box size of 0.05 and an increasing region size of 0.05°.

to 0.01°, or approximately 1 km. In addition, it will certainly be necessary to decimate the calculation down to these sizes to properly quantify magnitude five events (Wells and Coppersmith, 1994).

While larger strike–slip events such as Borrego Mountain or Landers do not appear to be particularly sensitive to the choice of exact epicenter, the smaller thrust events may rely on the correct epicenter location in order to define a cohesive rupture dimension. While this does not present difficulties for retrospective forecasting, as shown above, the advantage of prior knowledge of the actual epicenter does not exist for the anomalies in a prospective PI forecast. However, it is not necessary to test those locations for which there are no PI values present, i.e. where there are zeros in the PI matrix used to plot Fig. 2b. As an example, we performed this roughness calculation on one anomaly from the published forecast for the years 2000 to 2010 (Rundle et al., 2002), here reproduced in Fig. 2b. That chosen is the one centered on at 35.9° latitude, 120.5° longitude. This is not the exact location of the upcoming Parkfield earthquake in 2004, it lies approximately one box size to the northwest, at the site of two of that earthquake's largest aftershocks. It is, however, where the anomaly resides in that PI matrix, and there are no values associated with the actual epicenter.

Fig. 10 shows the results for this calculation. The calculation is performed for a PI box size of 0.05° and a roughness increment of 0.05°. The estimated rupture dimension is approximately 28 km, corresponding to an event of $M \sim 5.5$, slightly less than the $M \sim 6$ Parkfield earthquake that occurred in 2004. This calculation requires approximately 12 h on a standard workstation. While additional research is required in order to quantify the errors associated with this technique and the minimum box size required for an accurate magnitude estimate, it appears that it can be used to in a simple and effective manner to determine the approximate rupture dimension of those events forecast using the PI methodology. Finally, while this procedure could be easily automated in a forecasting methodology, the rupture dimensions should be inspected individually, and studied using additional seismic and geodetic techniques.

To conclude, research suggests that the PI method can be used to identify regions of localized seismicity variations associated with the nucleation of stress prior to the occurrence of large earthquakes. These localized regions appear to coalesce on the fault plane or planes, and define the rupture dimension of the upcoming event. A spatial map of the roughness index can give important information on the shape and orientation of this activation zone and provide insight into the potential mechanisms, reverse or strike–slip. Visual inspection of the roughness index, accompanied by detailed knowledge of the fault system and history, can assist in providing better estimates of the potential mechanisms. This technique can be used to quantify the size of large earthquakes in California over the past 40 years, including both thrust and strike–slip events, and shows promise for improved hazard forecasts. Future study will include those events included in intermediate-term forecasts for southern California.

Acknowledgments

This research was supported by the Southern California Earthquake Center. SCEC is funded by the NSF Cooperative Agreement EAR-0106924 and the USGS Cooperative Agreement 02HQAG0008. The SCEC contribution number for this paper is 916. Research by KFT is also supported by an NSERC Discovery grant. Research by JBR was funded by grant DE-FG02-04ER15568 from the US Department of Energy, Office of Basic Energy Sciences to the University of California, Davis. Research by WK was supported by USDOE/OBES grant DE-FG02-95ER14498 and W-7405-ENG-6 at LANL. WK would also like to acknowledge the hospitality and support of CNLS at LANL.

References

Beresnev, I.A., Atkinson, G.M., 2002. Source parameters of earthquakes in eastern and western North America based on finite-fault modeling. Bull. Seismol. Soc. Am. 92, 695–710.

Bowman, D.D., Ouillon, G., Sammis, C.G., Sornette, A., Sornette, D., 1998. An observational test of the critical earthquake concept. J. Geophys. Res. 103 (24), 359–372.

Dieterich, J., 1994. A constitutive law for rate of earthquake production and its application to earthquake clustering. J. Geophys. Res. 99, 2601–2618.

Dieterich, J.H., Cayol, V., Okubo, P., 2002. The use of earthquake rate changes as a stress meter at Kilauea volcano. Nature 408, 457–460.

Hauksson, E., Jones, L.M., Hutton, K., Eberhart-Phillips, D., 1993. The 1992 Landers earthquake sequence in California: seismological aspects. J. Geophys. Res. 98 (19), 835–858.

Hauksson, E., Jones, L.M., Hutton, K., 1995. The 1994 Northridge earthquake sequence in California: seismological and tectonic aspects. J. Geophys. Res. 100 (12), 335–355.

Holliday, J.R., Nanjo, K.Z., Tiampo, K.F., Rundle, J.B., Turcotte, D.L., 2005. Earthquake forecasting and its verification. Nonlinear Process. Geophys. 12 1607-7946/npg/2005-12-965.

Holliday, J., Chen, C., Tiampo, K.F., Rundle, J.B., Turcotte, D.L., Donnellan, A., in press. A RELM earthquake forecast based on pattern informatics, Seismological Research Letters.

Huang, Y., Saleur, H., Sammis, C., Sornette, D., 1998. Precursors, aftershocks, criticality and self-organized criticality. Europhys. Lett. 41, 43–49.

Jaume, S.C., Sykes, L.R., 1992. Evolving towards a critical point: a review of accelerating seismic moment/energy release prior to large and great earthquakes. Pure Appl. Geophys. 155, 279–306.

Joliffee, I.T., Stephenson, D.B., 2003. Forecast Verification. John Wiley and Sons, England.

Klein, W., Rundle, J.B., Ferguson, C.D., 1997. Scaling and nucleation in models of earthquake faults. Phys. Rev. Lett. 78, 3793–3796.

Main, I., 1996. Statistical physics, seismogenesis, and seismic hazard. Rev. Geophys. 34, 433–462.

Molchan, G.M., 1997. Earthquake predictions as a decision-making problem. Pure Appl. Geophys. 149, 233–247.

Mori, H., Kuramoto, Y., 1998. Dissipative Structures and Chaos. Springer-Verlag, Berlin.

Rundle, J.B., Klein, W., Tiampo, K.F., Gross, S., 2000. Linear pattern dynamics of nonlinear threshold systems. Phys. Rev., E 61, 2418–2432.

Rundle, J.B., Tiampo, K.F., Klein, W., Sá Martins, J., 2002. Self-organization in leaky threshold systems: the influence of near mean field dynamics & its implications for earthquakes, neurobiology and forecasting. Proc. Natl. Acad. Sci. U .S. A. 99 (Suppl. 1), 2463.

Tiampo, K.F., Rundle, J.B., McGinnis, S., Gross, S., Klein, W., 2002. Mean-field threshold systems and phase dynamics: an application to earthquake fault systems. Europhys. Lett. 60, 481–487.

Tiampo, K.F., Rundle, J.B., Klein, W., Sá Martins, J.S., Ferguson, C. D., 2003. Ergodic dynamics in a natural threshold system. Phys. Rev. Lett. 91, 238501.

Toda, S., Stein, R.S., Sagiya, T., 2002. Evidence from the AD 2000 Izu islands earthquake swarm that stressing rate governs seismicity. Nature 419, 58–61.

Wells, D.L., Coppersmith, K.J., 1994. Empirical relationships among the magnitude, rupture length, rupture width, rupture area, and surface displacement. Bull. Seismol. Soc. Am. 84, 974–1002.

Zechar, J.D., Jordan, T.H., 2005. Evaluation techniques for alarm-based forecasts. EOS, Trans. AGU (Fall meeting).